Accepted version

This is the author's version of the work. It is posted here for personal use, not for redistribution. The definitive version will be published in Nature Climate Change on Vol. 7, November issue.

Weakening of the North American monsoon with global warming

Salvatore Pascale[1,2,*] William R. Boos[3], Simona Bordoni[4], Thomas L. Delworth[2], Sarah B. Kapnick[2], Hiroyuki Murakami[1,2], Gabriel A. Vecchi[5], Wei Zhang[6]

[1] *Atmospheric and Oceanic Sciences Program, Princeton University, Princeton, NJ 08540, USA*

[2] *Geophysical Fluid Dynamics Laboratory/NOAA, Princeton, NJ 08540, USA*

[3] *Department of Earth and Planetary Science, University of California, Berkeley, and Climate and Ecosystem Sciences Division, Lawrence Berkeley National Laboratory, Berkeley, CA 94720, USA*

[4] *California Institute of Technology, Pasadena, CA 91125, USA*

[5] *Department of Geosciences, Princeton University, Princeton, NJ 08544,USA*

[6] *IIHR-Hydroscience and Engineering, The University of Iowa, Iowa City, IA 52242, USA*

[*] ***Corresponding author's address***: Princeton University, and NOAA/Geophysical Fluid Dynamics Laboratory, Princeton, New Jersey 08540, USA

E-mail: Salvatore.Pascale@noaa.gov

Previously at: California Institute of Technology, Pasadena, California 91125, USA

Future changes in the North American monsoon, a circulation system that brings abundant summer rains to vast areas of the North American Southwest [1, 2], could have significant consequences for regional water resources [3]. How this monsoon will change with increasing greenhouse gases, however, remains unclear [4, 5, 6], not least because coarse horizontal resolution and systematic sea surface temperature biases limit the reliability of its numerical model simulations [5, 7]. Here we investigate the monsoon response to increased atmospheric carbon dioxide (CO_2) concentrations using a 50 km-resolution global climate model which features a realistic representation of the monsoon and its synoptic-scale variability [8]. It is found that the monsoon response to CO_2 doubling is sensitive to sea surface temperature biases. When minimising these biases, the model projects a robust reduction in monsoonal precipitation over the southwestern United States, contrasting with previous multi-model assessments [4, 9]. Most of this precipitation decline can be attributed to increased atmospheric stability, and hence weakened convection, caused by uniform sea surface warming. These results suggest improved adaptation measures, particularly water resource planning, will be required to cope with projected reductions in monsoon rainfall in the American Southwest.

State-of-the-art general circulation models (GCMs) forced with greenhouse gas emission scenarios project a reduction of annual precipitation over a broad area of North America south of 35°N [10]. While wintertime precipitation is robustly projected to decline in this region due to a poleward expansion of the subtropical dry zones [11], summertime precipitation projections remain uncertain. This is due to a weak consensus across GCMs [10] and incomplete comprehension of the mechanisms through which global warming will impact the summertime North American monsoon (NAM). The NAM is shaped by both the complex regional geography (Supplementary Fig. 1) and remote larger-scale drivers [2, 12], which makes its simulation challenging [7, 13]. GCMs project a June-July reduction and a September-October increase in precipitation in the monsoon region [4, 9]. This early-to-late redistribution of rainfall has been conjectured to arise from two competing mechanisms [14]: a stronger tropospheric stability due to a remote sea surface temperature (SST) rise in spring that persists through early summer (a remote mechanism); and increased evaporation and near-surface moist static energy, driven by larger radiative fluxes at the surface (a local mechanism). The local mechanism is speculated to overcome the stabilizing effect of remote SST rise at the end of the summer [9]. However, the coarse horizontal resolution and existence of SST biases in coupled GCM simulations raise the question of how reliable such projections are for the NAM, which involves interactions across many spatial and temporal scales [12].

Horizontal resolution is critical for adequately representing the NAM in models. It has been recently shown [8] that GCMs with horizontal grid spacing coarser than 100 km (as most models participating in the Coupled Model Intercomparison Project, Phase 3 and 5, CMIP3 and CMIP5) do not accurately resolve the summertime low-level flow along the Gulf of California (GoC), with detrimental impacts on simulated precipitation in parts of the southwestern U.S. [1, 2]. For this reason, limited-area regional climate models have been used, suggesting drying of the monsoon region with warming [5]. Yet regional climate models lack two-way coupling with the larger-scale circulation and suffer from inherent boundary condition biases [15], making them a questionable tool for studying the climate change response.

GCM simulations of North American climate are affected by SST biases. In particular, negative SST anomalies in the North Atlantic can substantially influence the North Atlantic subtropical high through the upstream influence of a Gill-type Rossby wave response [16, 17, 18]. This results in unrealistically strong easterly low-level moisture flux across the Caribbean region, causing the well-known monsoon retreat bias, i.e., excessive monsoonal precipitation in the fall [7, 13]. These biases are thus a substantial source of uncertainty for the projected NAM response to CO_2 forcing.

To address these issues, here we investigate the response of the NAM to increased CO_2 and its sensitivity to both horizontal resolution and SST biases with the high resolution ($0.5^\circ \times 0.5^\circ$ in the land/atmosphere) Forecast-Oriented Low Ocean Resolution (FLOR) model [19, 20], developed at the National Oceanic and Atmospheric Administration (NOAA) Geophysical Fluid Dynamics Laboratory (GFDL). In addition to the standard configuration, the model can be run at coarser horizontal resolution (LOAR, $2^\circ \times 2^\circ$ in the land/atmosphere) or in a flux-adjusted version (FLOR-FA; see Methods).

Compared to LOAR, increased horizontal resolution in FLOR allows for a better representation of the fall retreat at the end of the warm season (Fig. 1f) and a more realistic pattern of near-surface moist static energy (Supplementary Fig. 2). FLOR also better resolves the seasonal cycle of low-level moisture flux along the GoC (Supplementary Fig. 3) and synoptic-scale variability within the monsoon [8]. These factors combine to create a more realistic simulation of the spatial pattern of mean rainfall (Fig. 1d) and the seasonal evolution of rainfall (Fig. 1f).

To assess the impact of SST biases [7, 13], we contrast the free-running coupled FLOR with its flux-adjusted version, FLOR-FA. The flux adjustment adds a modification term to surface fluxes of enthalpy, momentum, and freshwater, reducing SST biases in the basic state (Supplementary Fig. 4b), and leading to a realistic GoC SST annual cycle (Supplementary Fig. 5). Globally, flux adjustment improves the simulations of tropical cyclones [20], trade winds, dry zones in the Pacific, and El Niño [21]. Specifically to the NAM, one important improvement is the more realistic representation of the monsoon retreat (Fig. 1f). Other regional improvements include better representation of the high near-surface moist static energy along the GoC (Supplementary Fig. 2e), the GoC low-level jet (Supplementary Fig. 3), the Caribbean low-level jet, and the East Pacific Intertropical Convergence Zone. These results quantify that the separate impacts of both increased horizontal resolution and SST bias reduction enhance the simulation of the present-day NAM. The improvements seen in FLOR-FA suggest that this model is an excellent tool for investigations of the monsoon response to climate change.

When atmospheric CO_2 concentration is doubled ($2CO_2$_FLOR-FA vs. CTRL_FLOR-FA; Table 1), no statistically significant change is seen in mean June precipitation over the NAM region (Fig. 2a). A significant rainfall reduction is instead observed during July-August both in the core NAM region south of 28°N and in its northern edge north of 28°N (Supplementary Fig. 6). Because of the large difference in mean summertime precipitation, this drying is substantial in percentage terms primarily in the northern edge of the monsoon (~40%), becoming increasingly smaller south of 28°N (Fig. 2b). The drying persists – albeit weakened – over Arizona and northwestern Mexico during September-October, with no significant precipitation changes seen along the monsoon coastal regions (Fig. 2c). Similar results are found in a second ensemble member, and in additional runs at 25 km atmospheric horizontal resolution (not shown). These trends are in line with observations, which suggest that precipitation has decreased in Arizona in recent decades [22].

What determines the precipitation reduction over land during the mature monsoon season? We answer this question by estimating changes in the vertical buoyancy [23]

$$b = h_{10m} - h^* \tag{1}$$

induced by temperature and specific humidity changes. Here h_{10m} is the near-surface moist static energy and h^* the saturation moist static energy (see Methods). Fig. 3 illustrates changes in buoyancy and cumulus convective mass flux under doubled CO_2 concentrations following a transect from the tropical eastern Pacific across the Sierra Madre Occidental into the southwestern U.S. (Fig. 1a). In June, convection is mostly unchanged over the western slopes of the Sierra Madre Occidental and south of 32°N, consistent with modest, insignificant changes in vertical stability (Fig. 3a, d). In July-August, buoyancy decreases substantially between the lifted condensation level and the level of free convection over the most actively convecting regions on the Sierra Madre Occidental western slopes (Fig. 3b).

Consistently, cumulus convective mass fluxes weaken substantially over the Sierra Madre Occidental western slopes (10-30%) and elevated terrain in Arizona (25-50%; Fig. 3e). In September-October, the region of negative buoyancy differences narrows and disappears almost everywhere except north of 30°N. These patterns are consistent with those of convective mass flux changes (Fig. 3c,f).

Importantly, when SST biases are not substantially reduced (i.e., 2CO_2 FLOR vs. CTRL_FLOR), the response to CO_2 doubling is different (Fig. 2d-f), with a drier (20-30% rainfall reduction) June over both the southwestern U.S. and most of western Mexico (Supplementary Fig. 6), a substantially unaffected July-August (statistically insignificant differences), and a more pronounced tendency for larger rainfall rates along the coastal areas of western Mexico in September-October. This is consistent with the progressive increase from June to October in evaporation anomalies (Supplementary Fig. 7a-f) and decrease in sensible heat flux anomalies (Supplementary Fig. 7g-l). The changes evident in FLOR without flux adjustment follow the consensus based on CMIP3 and CMIP5 model assessments [4, 14, 9], which invokes a late summer evaporation increase – and with it a near-surface moist static energy increase – that balances the larger radiative fluxes at the surface. This compensation results in the suppression or even reversal of the early summer rainfall reduction (local mechanism). This similarity between FLOR and most of the CMIP5 models may be due indeed to their similar SST biases [16].

This picture is notably different in the southwestern U.S. and northwestern Mexico when SST biases are reduced (2CO_2_FLOR-FA vs. CTRL_FLOR-FA): the strongest rainfall decrease occurs in July-August (Fig. 2b) rather than in June. This more persistent drying in FLOR-FA reduces soil moisture availability and evaporation; hence, the local mechanism cannot reverse the drying, which persists until late summer. SST biases can thus substantially alter the intensity and effectiveness of the local mechanism [14, 9], leading to a change in the sign of the monsoon response to CO_2 forcing. One caveat is that the northernmost

GoC is not resolved in FLOR [8]; this may artificially reduce precipitation in the Southwest U.S. [24] and weaken the impact of the local mechanism during the late summer season.

The sensitivity of simulated rainfall changes to SST bias raises the question of how robust the projections shown in Fig. 2-3 are and what is the main driver of rainfall change. Although tropical precipitation changes produced by greenhouse gas warming are expected to be locally correlated with SST changes [25], it has been argued that the precipitation response over land is insensitive to patterns of SST change [26]. To understand the cause of our simulated precipitation changes, we use additional FLOR simulations in which SSTs are relaxed to a prescribed distribution (Table 1): (1) CLISST, where SSTs are relaxed to climatological 1971-2012 observed values; (2) $2CO_2$, where CO_2 concentration is doubled and SSTs are relaxed to climatological values as in CLISST; (3) +2K, where SSTs are relaxed to climatological values augmented by a uniform 2 K anomaly; (4) $2CO_2$_+2K, which is a combination of +2K and $2CO_2$; and (5) $2CO_2$_pattern, where CO_2 concentration is doubled and SSTs are relaxed to climatological values augmented by a nonuniform anomaly pattern derived from the long-term $2CO_2$ FLOR experiment, with global mean warming of +2.1 K. As shown in Fig. 4, the July-October NAM drying is in large part reproduced by $2CO_2$_pattern. Direct CO_2 forcing [27] causes a significant increase in June precipitation due to land and lower-troposphere warming [28], and compensates for the drying effect of SST rise. Although a uniform +2K warming generally increases convective inhibition over land and decreases precipitation, the spatial structure of the SST rise ($2CO_2$_pattern minus $2CO_2$_+2K) provides an important contribution to the total changes, as it leads to an additional and substantial reduction of rainfall (Fig. 4b). This additional drying is explained by the impact of spatial variations in the SST rise, characterized by enhanced near-equatorial warming and off-equatorial relative cooling in the eastern subtropical Pacific (Fig. 4c). As a consequence, subtropical subsidence intensifies as the sea surface warms more at the equator than in the subtropics. This response is in line with the “warmer-get-wetter” paradigm [25]; here we highlight the potential consequences of this response for the NAM region.

The strong sensitivity of the NAM response to SST biases shows that these may be a large source of uncertainty for regional hydroclimate change [29]. Here we demonstrate that, when SST biases are reduced, a CO_2 increase causes a reduction of summertime precipitation in the NAM region, especially over northwestern Mexico and the southwestern U.S. ($\sim$40%). These precipitation reductions are driven by the global mean SST rise, but, unlike what is seen in other tropical and subtropical land regions [26], they are substantially amplified by sea surface warming patterns. Interestingly, direct CO_2 radiative forcing [27, 28] has a negligible impact on the NAM, a circumstance that, along with the high interannual and interdecadal variability of NAM rainfall [2], may explain the difficulty to detect rainfall trends from historical observations [30].

Although our results are based on a single climate model, this model is integrated in multiple configurations and has a highly realistic representation of the monsoon compared to CMIP models. Our results highlight the possibility of a strong precipitation reduction in the northern edge of the monsoon in response to warming, with potential consequences for regional water resources, agriculture and ecosystems [3]. In addition to this mean precipitation response, changes in precipitation extremes [31] with warming will also have a significant impact in the monsoon region's hydrology. We will explore them in future studies. Further study of the sensitivity to key parameterized processes such as cumulus convection and land surface physics will improve understanding of the monsoon response. Additional progress is within reach, as increasing horizontal resolution in state-of-the-art GCMs will soon allow new comparative and idealized studies in this critical region.

References

[1] Adams D. K. and A. C. Comrie. The North American monsoon. *Bull. Amer. Meteor. Soc.*, 78:2197–2213, 1997.

[2] Higgins R. W., Y. Yao, and X. L. Wang. Influence of the North American monsoon system on the U.S. summer precipitation regime. *J. Climate*, 10:298–306, 1997.

[3] Ray A. J., G. M. Garfin, M. Wilder, M. Vasquez-León, M. Lenart, and A. C. Comrie. Applications of monsoon research: opportunities to inform decision making and reduce regional vulnerability. *J. Climate*, 20:1608–1627, 2007.

[4] Cook B. I. and R. Seager. The response of the North American monsoon to increased greenhouse gas forcing. *J. Geophys. Res.*, 118(4):1690–1699, 2013.

[5] Bukovsky M. S., C. M. Carrillo, D. J. Gochis, D. M. Hammerling, R. R. McCrary, and L. O. Mearns. Toward assessing NARCCAP regional climate model credibility for the North American monsoon: Future climate simulations. *J. Climate*, 28:6707–6728, 2015.

[6] Meyer J. D. D. and J. Jin. The response of future projections of the North American monsoon when combining dynamical downscaling and bias correction of CCSM4 output. *Climate Dyn.*, 49:433–447, 2017.

[7] Geil K. L., Y. L. Serra, and X. Zeng. Assessment of CMIP5 model simulations of the North American monsoon system. *J. Climate*, 26:8787–8801, 2013.

[8] Pascale S., S. Bordoni, S. B. Kapnick, G. A. Vecchi, L. Jia, T. L. Delworth, S. Underwood, and W. Anderson. The Impact of horizontal resolution on North American monsoon Gulf of California moisture surges in a suite of coupled global climate models. *J. Climate*, 29:7911–7936, 2016.

[9] Seth A., S. A. Rauscher, M. Rojas, A. Giannini, and S. J. Camargo. Enhanced spring convective barrier for monsoons in a warmer world? *Clim. Chang.*, 104:403–414, 2011.

[10] Maloney E. D., S. J. Camargo, E. Chang, B. Colle, R. Fu, K. L. Geil, Q. Hu, X. Jiang, N. Johnson, K. B. Karnauskas, J. Kinter, B. Kirtman, S. Kumar, B. Langenbrunner, K. Lombardo, L. N. Long, A. Mariotti, J. E. Meyerson, K. C. M, J. D. Neelin, Z. Pan, R. Seager, Y. Serra, A. Seth, J. Sheffield, J. Stroeve, J. Thibeault, S.-P. Xie, C. Wang, B. Wyman, and M. Zhao. North American climate in CMIP5 experiments: Part III:

Assessment of twenty-first-century projections. *J. Climate*, 27:2230–2270, 2014.

[11] Seager R. and G. A. Vecchi. Greenhouse warming and the 21st century hydroclimate of southwestern North America. *Proc. Natl. Acad. Sci. (USA)*, 107:21277–21282, 2010.

[12] Pascale S. and S. Bordoni. Tropical and extratropical controls of Gulf of California surges and summertime precipitation over the southwestern United States. *Mon. Wea. Rev.*, 144:2695–2718, 2016.

[13] Liang X.-Z., J. Zhu, K. E. Kunkel, M. Ting, and J. X. L. Wang. Do CGCMs simulate the North American monsoon precipitation seasonal-interannual variability? *J. Climate*, 21:4424–4448, 2008.

[14] Giannini A. Mechanisms of climate change in the semiarid African Sahel: The local view . *J. Climate*, 23:743–756, 2010.

[15] Lorenz P. and D. Jacob. Influence of regional scale information on the global circulation: A two-way nesting climate simulation. *Geophys. Res. Lett.*, 32:L18706, 2005.

[16] Wang C., L. Zhang, S.-K. Lee, L. Wu, and C. R. Mechoso. A global perspective on CMIP5 climate model biases. *Nature Climate Change*, 4:201–205, 2014.

[17] Sutton R. T. and D. L. R. Hodson. Climate response to basin-scale warming and cooling of the North Atlantic ocean. *J. Climate*, 20:891–907, 2006.

[18] Kushnir Y., R. Seager, M. Ting, N. Naik, and J. Nakamura. Mechanisms of tropical Atlantic SST influence on North American precipitation variability. *J. Climate*, 23:5610–5628, 2010.

[19] Delworth T. L., A. Rosati, W. Anderson, A. J. Adcroft, V. Balaji, R. Benson, K. Dixon, S. M. Griffies, H.-C. Lee, R. C. Pacanowski, G. A. Vecchi, A. T. Wittenberg, F. Zeng, and R. Zhang. Simulated climate and climate change in the GFDL CM2.5 high-resolution coupled climate model. *J. Climate*, 25:2755–2781, 2012.

[20] Vecchi G. A., T. Delworth, R. Gudgel, S. Kapnick, A. Rosati, A. T. Wittenberg, F. Zeng, W. Andersona, V. Balaji, K. Dixon, L. Jia, H.-S. Kim, L. Krishnamurthy, R. Msadek,

W. F. Stern, S. D. Underwood, G. Villarini, X. Yang, and S. Zhang. On the seasonal forecasting of regional tropical cyclone activity. *J. Climate*, 27:7994–8016, 2014.

[21] Manganello J.V. and B. Huang. The influence of systematic errors in the Southeast Pacific on ENSO variability and prediction in a coupled GCM. *Clim. Dyn.*, 32:1015–1034, 2009.

[22] Luong T. M., C. L. Castro, H.-I Chang, T. Lahmers, D. K. Adams, and C. A. Ochoa-Moya. The more extreme nature of North American monsoon precipitation in the southwestern U.S. as revealed by a historical climatology of simulated severe weather events. *J. Appl. Meteor. Climatol.*, pages doi.org/10.1175/JAMC–D–16–0358.1, in press, 2017.

[23] Randall D. An introduction to the global circulation of the atmosphere. Princeton University, Princeton, New Jersey, 456 pp, 2015.

[24] Mitchell D. L., D. Ivanova, R. Rabin, T. J. Brown, and K. Redmond. Gulf of California sea surface temperatures and the North American monsoon: mechanistic implications from observations. *J. Climate*, 15:2261–2281, 2002.

[25] Xie S.-P., C. Deser, G.A. Vecchi, J. Ma, H. Teng, and A.T. Wittenberg. Global warming pattern formation: Sea surface temperature and rainfall. *J. Climate*, 23:966–986, 2010.

[26] Chadwick R. Which aspects of CO_2 forcing and SST warming cause most uncertainty in projections of tropical rainfall change over land and ocean? *J. Climate*, 29:2493–, 2016.

[27] Bony S., G. Bellon, D. Klocke, S. Sherwood, S. Fermepin, and S. Denvil. Robust direct effect of carbon dioxide on tropical circulation and regional precipitation. *Nature Geoscience*, 22:4213–4227, 2013.

[28] Richardson T. B., P. M. Forster, T. Andrews, and D. J. Parker. Understanding the rapid precipitation response to CO_2 and aerosol forcing on a regional scale. *J. Climate*, 29:583–594, 2016.

[29] Zhou Z.-Q. and S.-P. Xie. Effects of climatological model biases on the projection of

tropical climate change. *J. Climate*, 28:9909–9917, 2015.

[30] Anderson B. T., J. Wang, G. Salvucci, S. Gopal, and S. Islam. Observed trends in summertime precipitation over the southwestern United States. *J. Climate*, 23:1937–1944, 2010.

[31] Pfahl S., P. A. O'Gorman, and E. M. Fischer. Understanding the regional pattern of projected future changes in extreme precipitation. *Nature Climate Change*, 7:423–427, 2017.

Methods

Experiments. We use the NOAA GFDL coupled Forecast-Oriented Low Ocean Resolution (FLOR) model [20], derived from the GFDL Coupled Model version 2.5 (CM2.5) [19]. CM2.5 features a $0.5^\circ \times 0.5^\circ$ atmospheric horizontal resolution with 32 vertical levels and has been successfully used for studies of regional hydroclimate change [1, 2]. FLOR is identical to CM2.5 but features a coarser ocean horizontal resolution ($1^\circ \times 1^\circ$ versus $0.25^\circ \times 0.25^\circ$). The land model component is the Land Model, version 3 [3], with a horizontal resolution equal to that of the atmospheric model. The sea ice model is the Sea Ice Simulator, version 1, as in [19]. A second model called LOAR (Low Ocean Atmosphere Resolution) is also used to test the impact of atmospheric horizontal resolution. The LOAR model has a horizontal atmospheric resolution of $2^\circ \times 2^\circ$ and is otherwise identical to FLOR [4].

As in most of CMIP5 models [16], FLOR features positive (negative) SST bias in the eastern (western) North Pacific and a negative SST bias in the North Atlantic (Supplementary Fig. 4). SST biases have a negative impact on simulations of the NAM in present-day climate [13] and are a source of uncertainty for projected changes in the tropics [29]. To reduce them, we use a flux-adjusted version of FLOR. In this configuration, which is otherwise identical to the standard FLOR configuration, fluxes of momentum, enthalpy and freshwater are "adjusted" to bring the model's climatology of SST, as well as surface wind stress and salinity, closer to observational estimates. We refer to this configuration as FLOR-FA. Details about the flux adjustment procedure can be found in [20]. FLOR-FA features reduced SST biases as compared to FLOR, especially in the Pacific and Atlantic oceans (Fig. S4). In both FLOR and FLOR-FA, long-term control simulations are performed with atmospheric CO_2 concentration held fixed at 1990 values. In the $2CO_2$ experiments, we increase CO_2 concentration at 1% per year starting from 1990 levels. After it has doubled (after approximately seventy years), we hold it constant and let the model run for additional two hundred years. In this experiment, the flux adjustment correction term remains the same as in the control run. As for freely-coupled models (i.e., developing systematic SST biases), the underlying assumption for applying the same adjustment correction under CO_2 forcing is that the emergent error in the SST climatology is the same in present and future climates.

Nudged-SST simulations. Mechanisms of NAM changes in response to CO_2 doubling are investigated with additional nudged-SST numerical simulations. In these simulations, simulated SSTs are restored toward a given field SST_0 while allowing high-frequency (i.e., on timescales smaller than the restoration timescale) SST fluctuations and ocean-atmosphere interactions. This is obtained by adding a restoration term $(SST_0 - SST)/\tau$ to the SST tendency equation:

$$d\,SST/dt = (d\,SST/dt)_C + (SST_0 - SST)/\tau \tag{2}$$

where $\tau = 10$ days is the restoration timescale and $(d\,SST/dt)_C$ the SST tendency as computed in the coupled model. Specifically, we perform five nudged-SST simulations in which: (1) SST_0 is the observed 1971-2012 climatological monthly-varying mean and CO_2 concentrations are held constant at 1990 values (CLISST); (2) SST_0 is the observed climatological monthly-varying SST mean and CO_2 concentration is doubled relative to 1990 values ($2CO_2$); (3) SST_0 is the observed climatological monthly-varying SST increased globally by 2K and CO_2 concentration is kept at 1990 values (+2K); (4) SST_0 is the observed climatological monthly-varying SST increased globally by 2K and CO_2 concentration is doubled relative to 1990 values ($2CO_2$_+2K); (5) SST_0 is the observed climatological monthly-varying SST plus a nonuniform SST anomaly taken from the long-term $2CO_2$ FLOR climatology and CO_2 is doubled relative to 1990 values ($2CO_2$ _pattern). Further details about these nudged-SST simulations and their purpose can be found in Table 1.

Observations. To validate the FLOR and FLOR-FA simulations, we use several observational datasets. For precipitation, we use the Global Precipitation Climatology Centre (GPCC) dataset [5]. GPCC is based on statistically interpolated *in situ* rain measurements and cover all land areas at monthly temporal resolution for the period 1901$-$2010. GPCC monthly precipitation data were obtained at $0.5° \times 0.5°$ horizontal resolution from the NOAA Physical Science Division Climate and Weather data website (www.esrl.noaa.gov/psd/data/). We use the Modern Era Retrospective-analysis for Research and Applications (MERRA) [6] for monthly and daily precipitation, near-surface moisture and winds. MERRA is a reanalysis with improved representation of the atmospheric branch of the hydrological cycle developed by NASA's Global Modeling and Assimilation Office (NASA Earth Observing System Data and Information System website: https://earthdata.nasa.gov/). Finally, the observed SST_0 field from the Met Office Hadley Centre Sea Ice and SST dataset [7] is used for the nudged-SST runs (Eq. 2) and to evaluate FLOR SST biases (Supplementary Fig. 4).

Buoyancy and convection diagnostics. The buoyancy of a saturated ascending air parcel, as measured by the difference between its temperature T_c and the temperature of the environment T, is proportional to the difference between the saturation moist static energy of the environment and the moist static energy of the ascending cloudy air [23]:

$$c_p\,(T_c - T) = \frac{h_c - h^*}{1+\gamma}, \tag{3}$$

where $h = c_p\,T + g\,z + L\,q$ is the moist static energy, h^* the saturation moist static energy, h_c the moist static energy of the ascending parcel, q is the specific humidity, g is the gravitational acceleration, $c_p = 1004$ J K^{-1} kg^{-1} is the isobaric specific heat of dry air, $L = 2.5 \times 10^6$ J kg^{-1}

latent heat of condensation, $q^*(T,p)$ the saturation specific humidity that we calculate using the August-Roche-Magnus formula [8] and $\gamma = (L/c_p)(\partial q^*/\partial T)_p$. Since the ascending parcel is lifted adiabatically from near surface, and thus lifted conserves its moist static energy, h_c is well approximated by the near-surface moist static energy, i.e. $h_{c_p} \approx h_{10m} = c_p\,T_{10m} + g\,z_{10m} + L\,q_{10m}$, here computed at the model's reference height z_{10m}=10 m. The parameter γ is positive and of order 1 [23], thus $h_{10m} - h^*$ is approximately twice the buoyancy value. To detect changes in the atmospheric convective instability, we estimate the buoyancy index $b = h_{10m} - h^*$ at each horizontal grid point x and vertical level p above the lifted condensation level, and then the buoyancy index anomaly Δb as:

$$\Delta b = \Delta(h_{10m} - h^*), \tag{4}$$

where the difference Δ is taken between the perturbed and the control simulation and positive (negative) values of b indicating upward (downward) acceleration.

Changes in the intensity of convection are assessed through changes in the diagnosed cumulus convective mass flux from the relaxed-Arakawa-Schubert scheme [9] employed in the GFDL models.

Statistical significance. We estimate statistical significance for differences shown in Fig. 2-3 and in Supplementary Fig. 7 using a two-sided Student's t-test at the 95% significance level. Confidence intervals for the mean differences shown in Fig. 4 are determined through applying 10^4 bootstrap resampling, as we randomly reshuffle the two time series (forced and control run) 10,000 times and the construct a probability distribution for the mean difference.

Data availability The data that support the findings of this study are available from the corresponding author upon request.

References

[1] Kapnick S. B., T. L. Delworth, M. Ashfaq, S. Malyshev, and P. C. D. Milly. Snowfall less sensitive to warming in Karakoram than in Himalayas due to a unique seasonal cycle. *Nature Geoscience*, 7:834 – 840, 2014.

[2] Delworth T. L. and F. Zeng. Regional rainfall decline in Australia attributed to anthropogenic greenhouse gases and ozone levels. *Nature Geoscience*, 7:583–587, 2014.

[3] Milly P. C. D., S. L. Malyshev, E. Shevliakova, K. A. Dunne, K. L. Findell, T. Gleeson, Z. Liang, P. Phillipps, R. J. Stouffer, and S. Swenson. An enhanced model of land water and energy for global hydrologic and earth-system studies. *J. Hydrometeor.*, 15:1739–1761, 2014.

[4] van der Wiel K., S. B. Kapnick, G. A. Vecchi, W. F. Cooke, T. L. Delworth, L. Jia, H. Murakami, S. Underwood, and F. Zeng. The resolution dependence of contiguous U.S. precipitation extremes in response to CO_2 forcing. *J. Climate*, 29:7991–8012, 2016.

[5] Schneider U., E. Becker, P. Finger, A. Meyer-Christoffer, M. Ziese, and B. Rudolf. GPCC's new land surface precipitation climatology based on quality-controlled in situ data and its role in quantifying the global water cycle. *Theoretical and Applied Climatology*, 115(1-2):15–40, 2013.

[6] Rienecker M. M., M. J. Suarez, R. Gelaro, R. Todling, J. Bacmeister, E. Liu, M. G. Bosilovich, S. D. Schubert, L. Takacs, G.-K. Kim, S. Bloom, J. Chen, D. Collins, A. Conaty, A. da Silva, W. Gu, J. Joiner, R. D. Koster, R. Lucchesi, A. Molod, T. Owens, S. Pawson, P. Pegion, C. R. Redder, R. Reichle, F. R. Robertson, A. G. Ruddick, M. Sienkiewicz, and J. Woollen. MERRA: NASA's Modern-Era Retrospective analysis for Research and Applications. *J. Climate*, 24:3624–3648, 2011.

[7] Rayner N., D. E. Parker, E. Horton, C. Folland, L. Alexander, D. Rowell, E. Kent, and A. Kaplan. Global analyses of sea surface temperature, sea ice, and night marine air temperature since the late nineteenth century. *J. Geophys. Res.*, 108:4407, 2003.

[8] World Meteorological Organization. *Technical Regulations*. Volume 1, WMO-No. 49, Geneva, 1988.

[9] Moorthi S. and M J Suarez. Relaxed Arakawa-Schubert: A parameterization of moist convection for general circulation models . *Mon. Wea. Rev.*, 120:978–1002, 1992.

Acknowledgements

S. P. was supported by the NOAA Climate and Global Change Postdoctoral Fellowship Program, administered by the University Corporation for Atmospheric Research, Boulder, Colorado and by the NOAA CICS grant - NA14OAR4320106. S.B. acknowledges support from the Caltech Davidow Discovery Fund. The authors thank Nathaniel Johnson and Honghai Zhang for comments on the manuscript.

Author contributions

S.P. designed the research and performed the analysis of the data. S. P. lead the writing with the assistance of S.B., S.B.K. and W.R.B.. S.P., W.R.B., S.B. and T.L.D. contributed to define the methods and to interpret the results. All authors took part in the discussion of the results and refined and improved the manuscript. H. M. and G. A. V. designed the model experiments. H. M. and W. Z. performed the simulations.

Competing financial interests

The authors declare no competing financial interests.

1 Figures

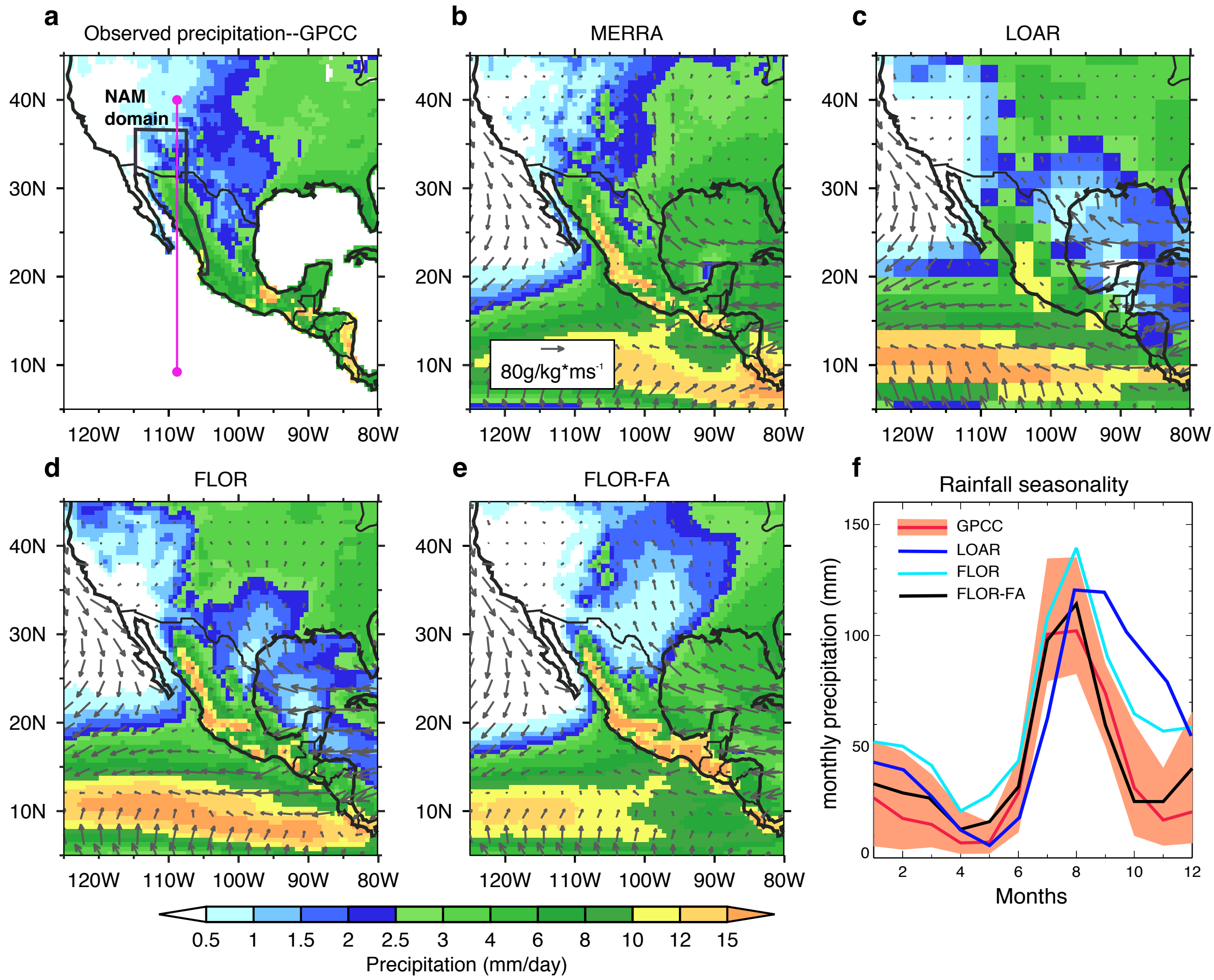

Figure 1: **High-resolution flux-adjusted models better capture regional features of the North American monsoon.** **a**, Time-mean (July-August) observed precipitation from GPCC (1971-2010). The blue contour delimits the area used for averaging over the North American monsoon in **f** and the magenta line the transect used for vertical cross-sections in Fig. 3. Precipitation (shading) and 10m-moisture flux (vectors) in **b**, MERRA reanalysis (1979-2010); **c**, LOAR, **d**; FLOR and **e**, FLOR-FA control runs (see Table 1 for description of experiments). **f**, Seasonal cycle of monthly precipitation averaged over the North American monsoon domain in observations and models. Shading denotes the interannual variability spread in observations.

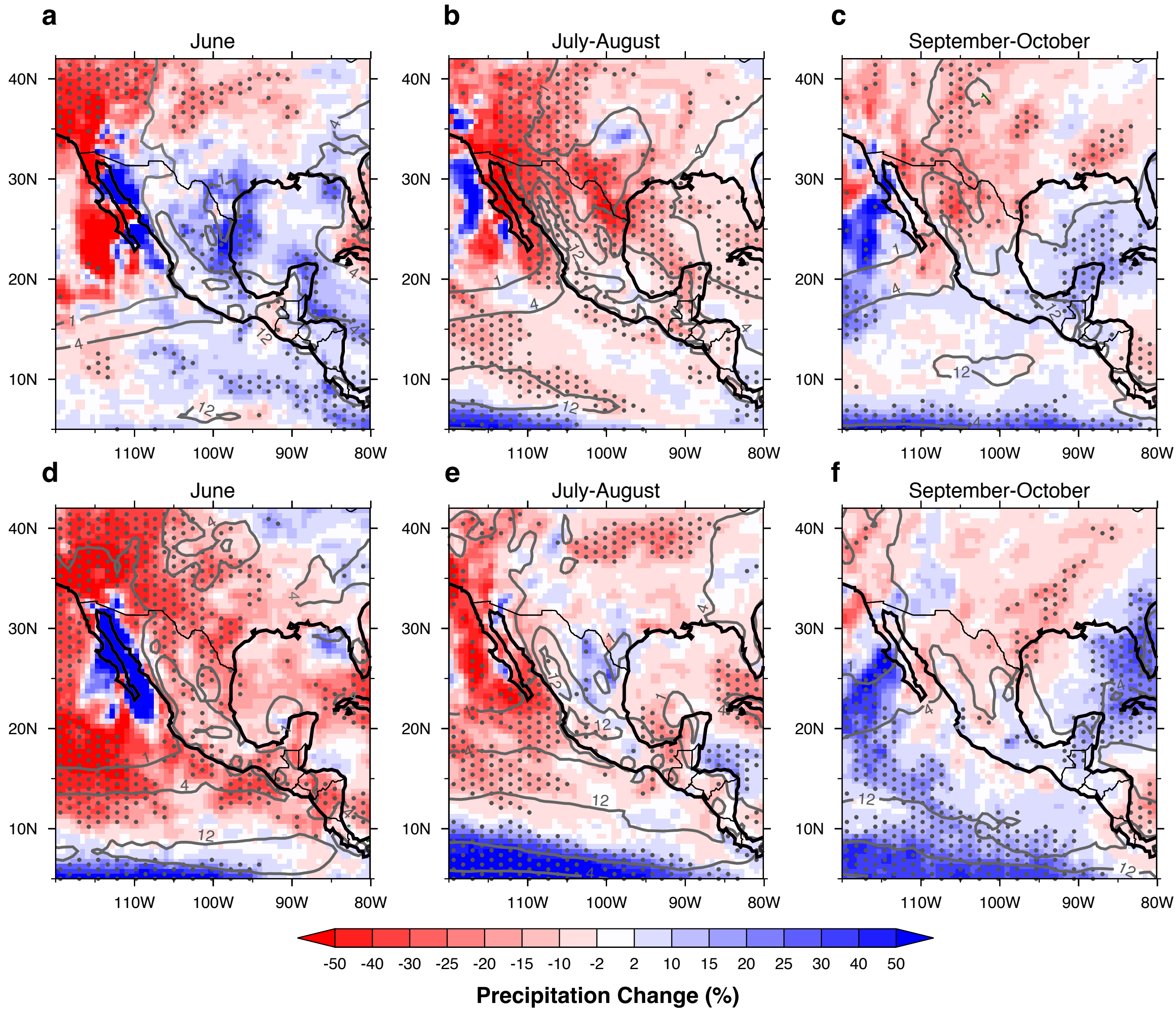

Figure 2: **Impact of increased CO_2 concentration and SST biases on the North American monsoon precipitation.** Percent precipitation change induced by CO_2 doubling in FLOR-FA simulations (%, color shading; 2CO_2_FLOR-FA minus CTRL_FLOR-FA) in **a** June, **b**, July-August, and **c**, September-October. **d**-**f**, As in **a**-**c** but for FLOR simulations (2CO_2_FLOR minus CTRL_FLOR). Grey contours denote climatological values of precipitation (mm/day) in the respective control runs. Stippling indicates regions where precipitation differences are statistically significant at the 5 % level on the basis of a t-test.

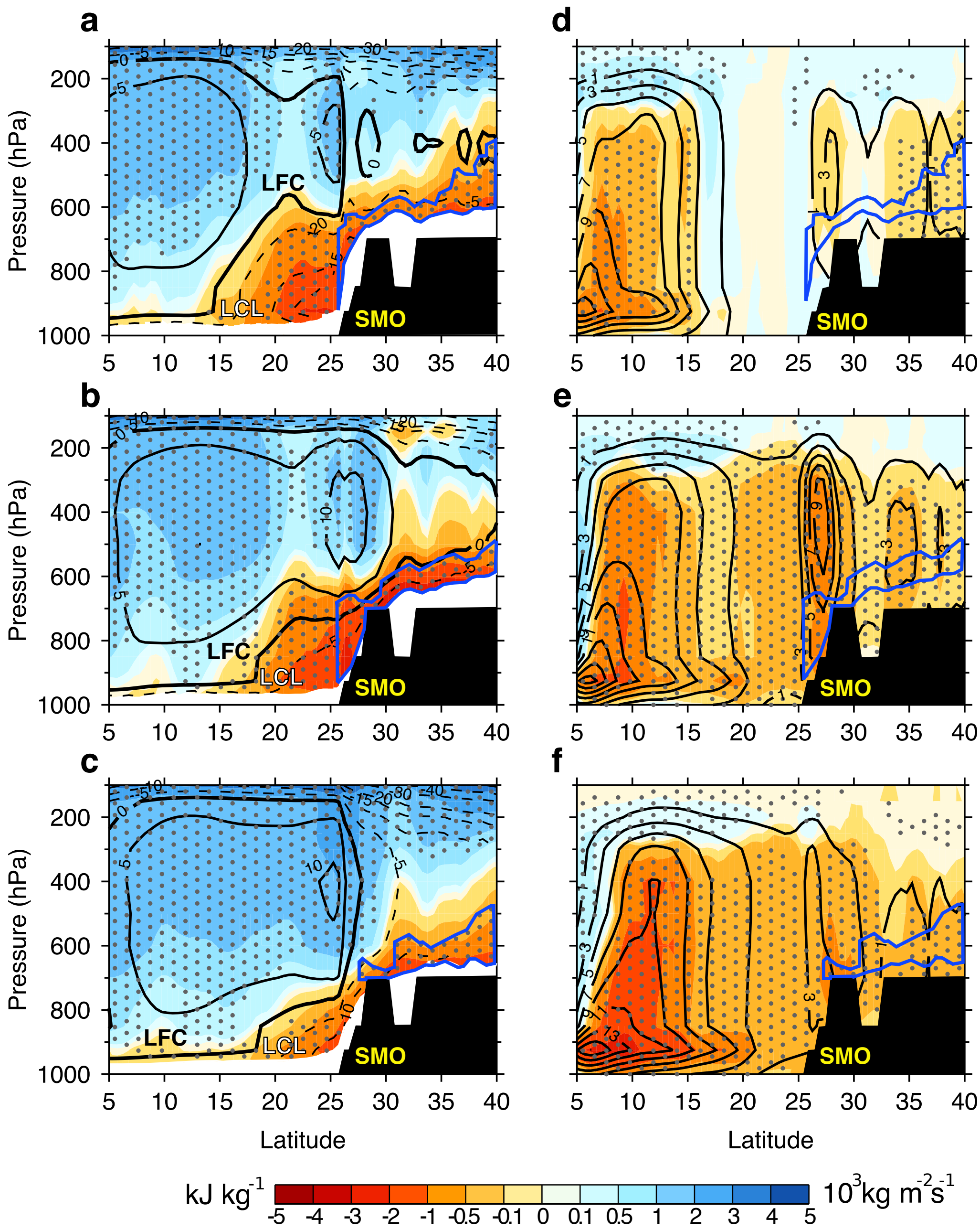

Figure 3: **CO_2-induced warming strengthens convective inhibition and weakens convection over land.** Difference in **a**, June, **b**, July-August and **c**, September-October mean buoyancy between doubled CO_2 and control FLOR-FA simulations (color shading; see Methods for details on buoyancy calculations). Stippling denotes statistical significance, black lines denote climatological values of buoyancy, LFC the level of free convection (zero buoyancy), and LCL the lifted condensation level. Buoyancy values below the LCL are not shown because the relationship between buoyancy and moist static energy does not hold for an unsaturated parcel. **d**-**f**, As in **a**-**c** but for the cumulus convective mass flux. The vertical transect is at 108°W (pink line in Fig. 1a) and intersects the Sierra Madre Occidental (SMO) at approximately 28°N. The blue line encircles areas over land where there is a significant buoyancy negative anomaly.

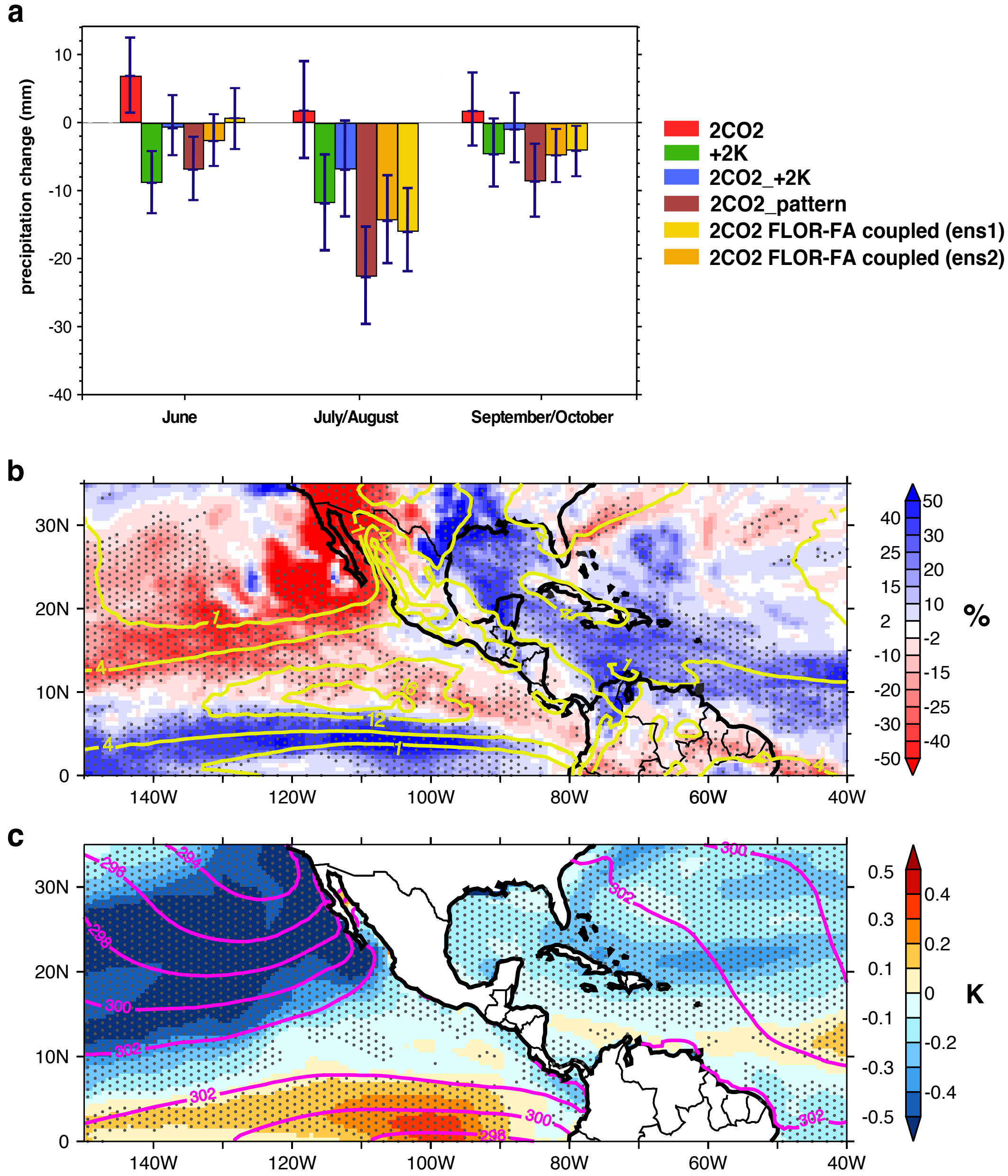

Figure 4: **Attribution of projected North American monsoon precipitation changes.** **a**, North American monsoon area-averaged (defined in Fig. 1) precipitation change attributed to each experiment (Table 1): $2CO_2$ (red), +2K (green), $2CO_2$_+2K (blue), $2CO_2$_pattern (brown) and the coupled $2CO_2$_FLOR-FA simulations (yellow for the ensemble member 1, orange for the ensemble member 2). Error bars denote the 95% confidence interval. **b**, Percent July precipitation change induced by patterns of SST anomalies ($2CO_2$_pattern minus $2CO_2$_+2K). Yellow contours denote the $2CO_2$_+2K climatology (mm/day). **c**, Areas of SST cooling and warming in the $2CO_2$_pattern run relative to the $2CO_2$_+2K run (uniform +2 K rise). Pink contours denote the $2CO_2$_+2K climatology (K). In both **b** and **c**, stippling indicates regions where precipitation differences are statistically significant at the 5 % level on the basis of a t-test.

List of Figures

Experiment	yrs	Radiative forcing/boundary conditions	Purpose
a) CTRL_FLOR	200	CO_2 constant at 1990 levels	Control run
b) CTRL_FLOR-FA	200	CO_2 constant at 1990 levels	Control run; Reduce SST biases
c) $2CO_2$ _FLOR	200	CO_2 doubles in 70 yrs, then constant	CO_2 forcing
d) $2CO_2$ _FLOR-FA	200	CO_2 doubles in 70 yrs, then constant	CO_2 forcing; Reduce SST biases
1) CLISST	50	Model SST restored to observed climatological (1971-2012) values	Remove SST biases
2) $2CO_2$	50	Model SST restored as in CLISST; atmospheric CO_2 concentration is doubled relative to 1990 levels	Impact of $2CO_2$ only
3) +2K	50	Model SST restored to observed climatological SST plus 2K (no warming pattern); CO_2 concentration is held at 1990 values	Impact of mean SST increase only
4) $2CO_2$_+2K	50	Model SST restored to observed climatological SST plus 2K (no warming pattern); CO_2 is doubled relative to 1990 levels	Combined impact of mean SST increase and $2CO_2$
5) $2CO_2$ _pattern	50	Model SST restored to observed climatological SST plus warming pattern from a long coupled $2CO_2$ run; CO_2 is doubled relative to 1990 levels	Combined impact of nonuniform SST anomaly and $2CO_2$

Table 1: Description of the coupled (a-d) and nudged-SST (1-5) experiments used in this study (see Methods for further details). Two ensemble members are available for experiments CTRL_FLOR, CTRL_FLOR-FA, $2CO_2$ _FLOR and $2CO_2$ _FLOR-FA.